IAC-13-C1.7.12

ACCESS TO MARS FROM EARTH-MOON LIBRATION POINT ORBITS: MANIFOLD AND DIRECT OPTIONS

Masaki Kakoi*
Purdue University, United States of America
kakoi@purdue.edu

Kathleen C. Howell†
Purdue University, United States of America
howell@purdue.edu

David Folta‡
NASA Goddard Space Flight Center, United States of America
david.c.folta@nasa.gov

This investigation is focused specifically on transfers from Earth-Moon L_1/L_2 libration point orbits to Mars. Initially, the analysis is based in the circular restricted three-body problem to utilize the framework of the invariant manifolds. Various departure scenarios are compared, including arcs that leverage manifolds associated with the Sun-Earth L_2 orbits as well as non-manifold trajectories. For the manifold options, ballistic transfers from Earth-Moon L_2 libration point orbits to Sun-Earth L_1/L_2 halo orbits are first computed. This autonomous procedure applies to both departure and arrival between the Earth-Moon and Sun-Earth systems. Departure times in the lunar cycle, amplitudes and types of libration point orbits, manifold selection, and the orientation/location of the surface of section all contribute to produce a variety of options. As the destination planet, the ephemeris position for Mars is employed throughout the analysis. The complete transfer is transitioned to the ephemeris model after the initial design phase. Results for multiple departure/arrival scenarios are compared.

I. INTRODUCTION

The far side of the lunar surface has held global interest for many years. One of the challenges in exploring the far side of the Moon is communications from/to the Earth. Multiple satellites are required to maintain a continuous link if a communications architecture relies only on lunar-centered orbits. Farquhar and Breakwell suggested an unusual three-body approach in response to this challenge in 1971.[1] This concept requires only one satellite by exploiting the characteristics of three-dimensional halo orbits in the vicinity of the Earth-Moon L_2 (EML_2) libration point. Unfortunately, this plan was never implemented due to a shortening of the Apollo program. However, interest in the exploration of the far side of the Moon has recently increased, particularly in the aftermath of the successful Artemis mission.[2] In addition, a new exploration strategy has recently emerged, that is, possibly establishing a space station in an EML_1/L_2 orbit and leveraging this station as a hub for the exploration of the asteroids and Mars.[3]

The potential of an EML_1/L_2 hub for further exploration is yet to be investigated extensively. To examine the feasibility, mission designers require an improved understanding of the dynamics that influence a transfer trajectory from EML_1/L_2 libration point orbits to possible destination objects, and the capability to produce such trajectories via a reasonably straightforward and efficient design process. Analysis concerning possible trajectories from EML_1/L_2 orbits to Mars is explored by applying dynamical relationships available as a result of formulating the problem in terms of multiple three-body gravitational environments.

II. PREVIOUS CONTRIBUTORS

Within the last decade, interest in a mission design approach that leverages the knowledge of dynamical systems theory (DST) has increased steadily amongst scholars and trajectory designers. Howell et al. examined the application of DST within a trajectory design

*Ph.D. Candidate, School of Aeronautics and Astronautics
†Hsu Lo Distinguished Professor of Aeronautics and Astronautics
‡Aerospace Engineer

process in the late 1990's.[4] The knowledge was actually applied to design the GENESIS mission trajectory, launched in 2001.[5,6] GENESIS was the first spacecraft for which the concept of invariant manifolds was directly applied to develop the actual path of the vehicle.[7] The successful return of the GENESIS spacecraft demonstrated that DST can be exploited for actual trajectory design in multi-body environments. In addition, scientific missions such as MAP and WIND relied on three-body dynamics for their successful trajectory designs around the similar time.[8,9]

As the result of a set of successful missions, interest in DST applications to trajectory design has increased and researchers have expanded their investigation to exploit DST and better understand the dynamics in the more complex four-body systems which consist of three gravitational bodies and one spacecraft. About 10 years ago, Gómez et al. introduced a methodology to design transfer trajectories between two circular restricted three-body systems by exploiting invariant manifold structures.[10,11] They modeled a four-body system by blending two CR3BPs. The focus of investigation on such system-to-system transfers was originally based on a Jovian moon system as well as spacecraft moving in the Sun-Earth-Moon neighborhood.[12–14] But, Gómez et al. demonstrated the potential exploitation of the CR3BP as a modeling tool to investigate four-body systems. Parker and Lo employed the planar model to design three-dimensional trajectories from Low Earth Orbits (LEO) to Earth-Moon L_2 halo orbits.[15] In addition, Parker also applied DST as a design tool to develop transfer strategies from LEOs to a broader range of EM halo orbits.[16–18] The investigation in the Sun-Earth-Moon system eventually was extended to transfers between libration point orbits in the Sun-Earth and Earth-Moon systems. Howell and Kakoi introduced a model with an inclination between the Earth-Moon and the Sun-Earth systems to design transfers between Earth-Moon L_2 halo orbits and Sun-Earth L_2 halo orbits.[19] Canalias and Masdemont extended the investigation to transfers between quasi-periodic Lissajous orbits in different systems, i.e., Earth-Moon and Sun-Earth.[20] In addition, transfer trajectory design methods between Earth-Moon and Sun-Earth systems have been investigated using various strategies as well.[16,18,21–23]

Dynamical systems theory has also been suggested as a design tool for interplanetary trajectory design.[24,25] However, since manifolds associated with the Sun-Earth libration point orbits do not intersect with manifolds in other Sun-Planet systems, such as Sun-Mars or Sun-Jupiter systems, different techniques have been developed for interplanetary transfer arcs. Alonso and Topputo et al. investigated techniques to link non-intersecting manifolds with an intermediate high energy trajectory arc.[26–28] Nakamiya et al. analyzed maneuver strategies at perigee and periareion for Earth-to-Mars transfers.[29,30] As alternatives to the high energy arcs, low-thrust arcs have also been investigated for transfers between the two systems[22,31–34]

The past investigations on the system-to-system transfer design strategies have successfully contributed numerous design techniques and insight into the four-body regime. However, interplanetary trajectory design techniques from the Earth-Moon libration point orbits warrants further examination.

III. SYSTEM MODEL

One of the most important trajectory design tools is a reasonable model of the system. The model must represent the physical system to a certain level of accuracy and offer the desired system characteristics, but the model must also be sufficiently simple such that mission designers can readily analyze the dynamics and interactions between various trajectories. The circular restricted three-body problem offers both the complexity and well-known manifold structures to represent the actual motion that designers can exploit.

III.I. Circular Restricted Three-Body Problem

A schematic of the fundamental circular restricted three-body problem (CR3BP) appears in Fig. 1. Primary bodies, P_1 and P_2, rotate about their mutual barycenter with a constant angular velocity. The masses of P_1 and P_2 are defined as m_1 and m_2. A massless body, P_3, moves under the gravitational influence of the primary bodies. An inertial frame is defined by a set of three orthogonal vectors $[\hat{X},\hat{Y},\hat{Z}]$. The unit vector $\hat{Z}$ aligns with the angular momentum vector for the motion of primary bodies. The unit vector $\hat{X}$ is defined on the plane of the motion of primary bodies. Then, the unit vector $\hat{Y}$ completes the right-handed triad. A set of three orthogonal vectors $[\hat{x},\hat{y},\hat{z}]$ defines a rotating frame in which the equations of motion are derived. The unit vector $\hat{x}$ is defined in the direction from P_1 toward P_2, and the unit vector $\hat{z}$ is aligned with $\hat{Z}$. Then, the unit vector $\hat{y}$ is a cross product of $\hat{z}$ and $\hat{x}$. Therefore, when the angle θ in Fig. 1 is 0°, $[\hat{X},\hat{Y},\hat{Z}]$ and $[\hat{x},\hat{y},\hat{z}]$ are identically aligned. The nondimensional mass ratio μ is defined as $\mu = \frac{m_2}{m_1+m_2}$. To represent a physical system such as a Sun-Planet system, the larger mass, i.e., mass of the Sun, is typically assigned to m_1 and the smaller mass, i.e., mass of planet, is assigned to m_2. Let the nondimensional locations of P_1 and P_2 with respect to the barycenter expressed in terms of the rotating frame to be $\bar{d}_1$ and $\bar{d}_2$ respectively. Distances are nondimensionalized utilizing the distance between primaries as the characteristic length, r^*. Consequently, the nondimensional vectors $\bar{d}_1$ and $\bar{d}_2$ are defined as $\bar{d}_1 = x_1\hat{x}$ and $\bar{d}_2 = x_2\hat{x}$, respectively. Then, the nondimensional mass ratio defines x_1 and x_2 as $x_1 = -\mu$ and $x_2 = 1-\mu$,

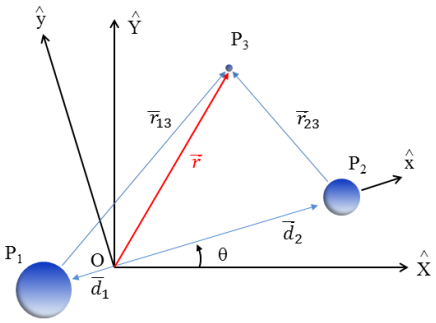

Fig. 1: Formulation of the Circular Restricted Three-Body Problem

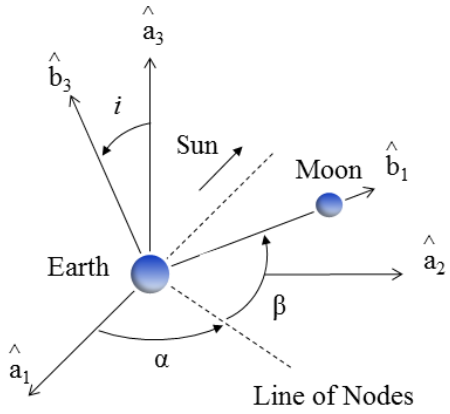

Fig. 2: Angle Definitions in the Three-Dimensional Model: Euler angle sequence body-two 3-1-3

respectively. The nondimensional location of P_3 with respect to the barycenter in the rotating frame is denoted as $\bar{r}$, and the nondimensional vector is expressed as $\bar{r} = x\hat{x} + y\hat{y} + z\hat{z}$. Also, the location of P_3 with respect to P_1 and P_2 is denoted as $\bar{r}_{13}$ and $\bar{r}_{23}$, respectively. Time is nondimensionalized by the mean motion of primaries, $n = \sqrt{\frac{G(m_1+m_2)}{r^{*3}}}$, where G is the universal gravitational constant whose value is approximately $6.67384 \times 10^{-11} \frac{m^3}{kg*s^2}$. Thus, the nondimensional angular velocity of the rotating system relative to the inertial frame is unity. Then, the scalar, second-order equations of motion for the CR3BP are,

$$\ddot{x} - 2\dot{y} - x = -(1-\mu)\frac{x-x_1}{r_{13}^3} - \mu\frac{x-x_2}{r_{23}^3}, \quad [1]$$

$$\ddot{y} + 2\dot{x} - y = -\left(\frac{1-\mu}{r_{13}^3} + \frac{\mu}{r_{23}^3}\right) y, \quad [2]$$

$$\ddot{z} = -\left(\frac{1-\mu}{r_{13}^3} + \frac{\mu}{r_{23}^3}\right) z. \quad [3]$$

Dots indicate derivatives with respect to the nondimensional time, and r_{13} and r_{23} are magnitudes of $\bar{r}_{13}$ and $\bar{r}_{23}$, respectively.

III.II. Blending CR3BPs

The circular restricted three-body problem has been successfully demonstrated as a powerful design tool to provide insight into the actual motion of a body in space such as a spacecraft or a comet.[35,36] Of course, the number and type of gravitational bodies for the design of some specific trajectory vary according to the spacecraft destination, and the CR3BP itself may not be sufficient to model the appropriate dynamical regime. Hence, the capability to model a system with more than two gravitational bodies is essential. One approach to model such a system that has been previously explored is a blending of CR3BPs. For example, a four-body system such as a Sun-Earth-Moon can be modeled by overlapping Sun-Earth and Earth-Moon systems at the common body, Earth. This technique can incorporate the difference in the orientation of the fundamental orbital planes of the two systems to enhance the level of accuracy. In Fig. 2, the location of the Moon is defined relative to the other bodies in the system. The rotating frame corresponding to the Sun-Earth system is expressed as a set of three orthogonal unit vectors $[\hat{a}_1, \hat{a}_2, \hat{a}_3]$. The Sun is in the direction corresponding to $-\hat{a_1}$. Another set of three orthogonal unit vectors $[\hat{b}_1, \hat{b}_2, \hat{b}_3]$ reflects the rotating frame of Earth-Moon system, and the orientation of $[\hat{b}_1, \hat{b}_2, \hat{b}_3]$ with respect to $[\hat{a}_1, \hat{a}_2, \hat{a}_3]$ is defined by the Euler angle sequence, body-two 3-1-3. The first angle α defines the orientation of the line of nodes with respect to $\hat{a}_1$. The second angle i defines the inclination of the lunar orbit plane with respect to the Earth orbit. The third angle β identifies the lunar location in the orbital plane relative to the line of nodes, i.e., ascending node.

A similar model formulation is possible to design interplanetary trajectories by blending a Sun-Earth system and a Sun-Planet system. For example, to design a trajectory from Earth to Mars, Sun-Earth and Sun-Mars systems are overlapped at the common body, i.e., the Sun. In this case, the inclination of Mars orbit is generally neglected since the inclination relative to the ecliptic plane is 1.51°, small compared to the lunar orbit inclination, 5.09°.[37] Then, the location of Mars with respect to the Sun-Earth rotating frame is defined by only one angle. This assumption simplifies the model and is generally adequate for a corrections process. However, the Mars orbit is more elliptic than the Earth orbit or the Moon orbit. The eccentricity of the Mars orbit is 0.0934 compared to 0.0167 and 0.0549 of the Earth orbit and the Moon orbit, respectively.[37] Therefore, the exploitation of a CR3BP for the Sun-Mars system reduces the level of accuracy as a model. However, the goal is an effective initial guess for the higher-fidelity model, i.e., one that can be transitioned while retaining similar characteristics. This investigation examines the viability of such a model.

III.III. Model for Transfers to Mars

To achieve a higher level of accuracy in the construction of a preliminary path, the ephemeris Mars locations are incorporated into the system model. Two

options are available for this Mars orbit model. The first option incorporates the Mars' gravitational force. The gravitational force from Mars is computed in an inertial frame, based on the location of a spacecraft as well as the epoch. Thus, the exploitation of the CR3BP is not trivial in this formulation. An alternative option is incorporating only the state information for the ephemeris locations of Mars. In this model, the Mars data is transformed into the Sun-Earth rotating frame and the trajectory design process is executed in the Sun-Earth system. This option allows incorporation of Mars' actual position into the CR3BP.

IV. MULTIPLE SHOOTING

Trajectory design requires the capability to link different types of arcs, including both two-body and three-body arcs, to meet mission requirements. The same type of corrections process is also employed to transition to a model of different fidelity or add new forces to an existing model. Thus, mission designers must be equipped with various design tools to link multiple arcs. One possible strategy to accomplish such a task is a multiple shooting method.[38] Such a numerical corrections scheme has been demonstrated to be useful in trajectory design.[39,40] A multiple shooting schematic is illustrated in Fig. 3. The black dots represent 6-D states estimated to be on a desirable path, that is, an initial guess. The states are denoted $\bar{x}_i$ where the subscript i is an index. Each $\bar{x}_i$ is comprised of position components as well as velocity components, e.g., $\bar{x}_1 = [r_{x1}, r_{y1}, r_{z1}, v_{x1}, v_{y1}, v_{z1}]$. Propagating a state, $\bar{x}_i$, over time, t_i, by means of function $\bar{f}$ yields the trajectory represented by a solid arc in the figure. As an initial guess, the state $\bar{x}_i$ does not, in fact, reach the desired state $\bar{x}_{i+1}$ after the propagation. The actual final state along each arc is denoted by $\bar{f}(\bar{x}_i, t_i)$, and it is defined by position components, $r^f_{xi}, r^f_{yi}, r^f_{zi}$ and velocity components, $v^f_{xi}, v^f_{yi}, v^f_{zi}$ as $\bar{f}(\bar{x}_i, t_i) = [r^f_{xi}, r^f_{yi}, r^f_{zi}, v^f_{xi}, v^f_{yi}, v^f_{zi}]$. The superscript f indicates the final state along arc i. If arcs are not linked, as in the figure, final states from the propagation, $\bar{f}(\bar{x}_i, t_i)$, and the following initial states $\bar{x}_{i+1}$ are modified to achieve a continuous trajectory. To achieve a continuous path, various types of corrections strategies could be applied. From among many options, a free-variable/constraint approach is employed. This corrections process is detailed in Pavlak.[41] A free variable vector, $\bar{X}$, and a constraint vector, $\bar{F}$, are defined as follows,

$$\bar{X} = [\bar{x}_1,\ t_1,\ \bar{x}_2,\ t_2,\ \bar{x}_3,\ t_3]^T, \quad [4]$$

$$\bar{F}(\bar{X}) = \left[\bar{x}_2 - \bar{f}(\bar{x}_1, t_1),\ \bar{x}_3 - \bar{f}(\bar{x}_2, t_2),\ \bar{x}_4 - \bar{f}(\bar{x}_3, t_3)\right]^T = \bar{0}, \quad [5]$$

where $\bar{X}$ is a column vector of free variables and $\bar{F}$ is a column vector of equality constraints. The superscript T indicates a transpose. Then, these constraints are achieved numerically by the iterative application of a vector Newton's method with the following update equation,

$$\bar{X}_{j+1} = \bar{X}_j - DF(\bar{X}_j)^{-1}\bar{F}(\bar{X}_j), \quad [6]$$

where $\bar{X}_j$ is a free variable vector at the j^{th} iteration and $DF(\bar{X}_j)$ is the Jacobian matrix. The Jacobian matrix is constructed as partial derivatives of the constraint vector with respect to the free variable vector evaluated at the j^{th} iteration. Generally, the number of free variables is larger than the number of constraints. Thus, $DF(\bar{X}_j)$ is not expected to be invertible. In this case, it is necessary to modify Equation [6] with a pseudo-inverse of $DF(\bar{X}_j)$, such that

$$\bar{X}_{j+1} = \bar{X}_j - DF(\bar{X}_j)^T[DF(\bar{X}_j) \cdot DF(\bar{X}_j)^T]^{-1}\bar{F}(\bar{X}_j), \quad [7]$$

to produce a minimum norm update. In this formulation, $DF(\bar{X}_j)$ is not required to be invertible.

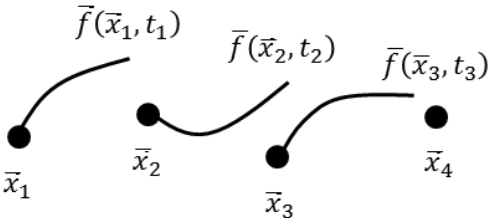

Fig. 3: Illustration of Multiple Shooting

Allowing maneuvers to link multiple arcs increases flexibility in the process. A maneuver application can be simply formulated by omitting velocity components from the specified constraint. For example, let the constraint vector for $\bar{f}(\bar{x}_2, t_2)$ be $\bar{F}_2$. Then, to allow a maneuver at $\bar{f}(\bar{x}_2, t_2)$, $\bar{F}_2$ is formulated as follows,

$$\bar{F}_2 = [r_{x3},\ r_{y3},\ r_{z3}]^T - [r^f_{x2},\ r^f_{y2},\ r^f_{z2}]^T = \bar{0}, \quad [8]$$

where r_{x3}, r_{y3}, and r_{z3} are position components corresponding to $\bar{x}_3$, and r^f_{x2}, r^f_{y2}, and r^f_{z2} are position components of $\bar{f}(\bar{x}_2, t_2)$. In this formulation, the magnitude of the maneuver is not regulated. However, since the amount of propellant is always limited, a means to constrain the maximum maneuver size is necessary. The magnitude of a maneuver, ΔV, at $\bar{f}(\bar{x}_2, t_2)$ is expressed in terms of velocity components of $\bar{x}_3$ and $\bar{f}(\bar{x}_2, t_2)$, v_{x3}, v_{y3}, v_{z3} and v^f_{x2}, v^f_{y2}, v^f_{z2}, respectively,

$$\sqrt{(v_{x3} - v^f_{x2})^2 + (v_{y3} - v^f_{y2})^2 + (v_{z3} - v^f_{z2})^2} = \Delta V. \quad [9]$$

Hence, an additional scalar constraint, $F_{\Delta V}$ to constrain the velocity difference between $\bar{x}_3$ and $\bar{f}(\bar{x}_2, t_2)$ is the following,

$$F_{\Delta V} = \sqrt{(v_{x3} - v^f_{x2})^2 + (v_{y3} - v^f_{y2})^2 + (v_{z3} - v^f_{z2})^2} - \Delta V = 0. \quad [10]$$

However, in this formulation, the partial derivatives possess a singularity when the velocity difference is very small. To avoid the singularity, Equation [9] is squared. Then, Equation [10] becomes as follows,

$$F_{\Delta V} = (v_{x3}-v_{x2}^f)^2+(v_{y3}-v_{y2}^f)^2+(v_{z3}-v_{z2}^f)^2-\Delta V^2 = 0. \quad [11]$$

The constraint $F_{\Delta V}$ actually specifies the ΔV level. Thus, to improve the application of the constraint $F_{\Delta V}$ to introduce flexibility, an inequality constraint is a better alternative. The inequality is formulated as an equality constraint by introducing a slack variable, η, and the new formulation is written,

$$\begin{aligned} F_{\Delta V} &= (v_{x3} - v_{x2}^f)^2 + (v_{y3} - v_{y2}^f)^2 + (v_{z3} - v_{z2}^f)^2 \\ &\quad -(\Delta V - \eta^2)^2 = 0. \end{aligned} \quad [12]$$

The slack variable η is squared such that ΔV - η^2 is always smaller than or equal to ΔV. Then, the final formulation with a scalar ΔV constraint at $\bar{x}_3$ is the following,

$$\bar{X} = [\bar{x}_1,\ t_1,\ \bar{x}_2,\ t_2,\ \bar{x}_3,\ t_3,\ \eta]^T, \quad [13]$$

$$\bar{F}(\bar{X}) = \left[\bar{F}_1,\ \bar{F}_2,\ \bar{F}_3,\ F_{\Delta V}\right]^T = \bar{0}, \quad [14]$$

where

$$\bar{F}_1 = \bar{x}_2 - f(\bar{x}_1, t_1), \quad [15]$$

$$\bar{F}_2 = [r_{x3},\ r_{y3},\ r_{z3}] - [r_{x2}^f,\ r_{y2}^f,\ r_{z2}^f], \quad [16]$$

$$\bar{F}_3 = \bar{x}_4 - f(\bar{x}_3, t_3), \quad [17]$$

$$\begin{aligned} F_{\Delta V} &= ((v_{x3} - v_{x2}^f)^2 + (v_{y3} - v_{y2}^f)^2 + (v_{z3} - v_{z2}^f)^2 \\ &\quad -(\Delta V - \eta^2)^2. \end{aligned} \quad [18]$$

The maximum maneuver size, ΔV, and an initial guess for η are required to solve for $\bar{F} = \bar{0}$. The initial guess for η is such that the scalar constraint is satisfied, $F_{\Delta V} = 0$.

V. MANEUVER-FREE TRANSFERS BETWEEN EARTH-MOON AND SUN-EARTH SYSTEMS

One possible scenario for a transfer from a three-dimensional Earth-Moon (EM) halo orbit to the planet Mars is the exploitation of unstable Sun-Earth (SE) manifolds. However, to utilize this option, it is necessary to transfer from an EM halo orbit to a manifold associated with a SE halo orbit. Even though different techniques for such transfers have been investigated by linking manifolds associated with EM halo orbits to those corresponding to SE halo orbits, it is still challenging to compute maneuver-free transfers between the Earth-Moon system and the Sun-Earth system. Thus, it is crucial to establish a general process to construct maneuver-free transfers for exploiting SE manifolds as a platform for departure to Mars.

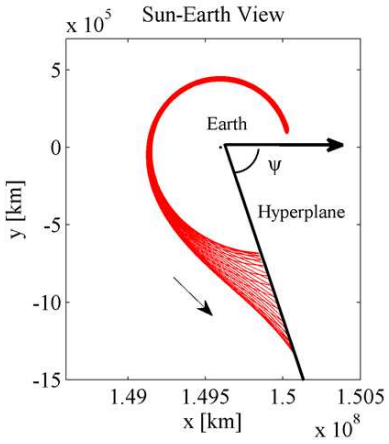

Fig. 4: Definition of ψ: It is measured from the SE x-axis in the counter-clockwise direction

V.I. Hyperplane and Reference Frame

A hyperplane is useful for computing halo-to-halo spacecraft transfers. In Fig. 4, the x-y projections of a hyperplane and Earth-Moon manifolds in red appear. The location of the hyperplane is defined by an angle ψ, and it is measured from the Sun-Earth x-axis in the counter-clockwise direction. State vectors corresponding to both Earth-Moon and Sun-Earth manifolds are projected onto the hyperplane; this projected information offers valuable insight for the computation of maneuver-free transfer paths. To visualize the projected information as phase plots, a new reference frame is defined on the hyperplane by a set of orthogonal unit vectors $[\hat{x}_{ref}, \hat{y}_{ref}, \hat{z}_{ref}]$. The intersection between the Sun-Earth x-y plane and the hyperplane defines $\hat{x}_{ref}$. The direction of $\hat{x}_{ref}$ is defined so that it becomes identical with $\hat{x}$ in the Sun-Earth system when ψ is equal to zero degrees. The unit vector $\hat{z}_{ref}$ is identical to the Sun-Earth $\hat{z}$. The cross product between $\hat{z}_{ref}$ and $\hat{x}_{ref}$ defines $\hat{y}_{ref}$. Position and velocity components expressed in terms of the hyperplane reference frame are represented as $[x_{ref}, y_{ref}, z_{ref}, \dot{x}_{ref}, \dot{y}_{ref}, \dot{z}_{ref}]$. Phase plots represented in this reference frame are exploited to discover the lunar location and the Sun-Earth Az value for a maneuver-free transfer from an Earth-Moon halo orbit with a specified Az value.

V.II. Phase Plots to Establish Orientation of Earth-Moon System

To achieve a maneuver-free transfer, the appropriate combination of all variables must be determined including α, β, ψ, EMAz, and SEAz. Although a very challenging task, the procedure to compute the appropriate values is simplified by exploiting the phase plots created by the projection of the appropriate states on a hyperplane that is essentially a two-dimensional space.

The location of a hyperplane is a key element in

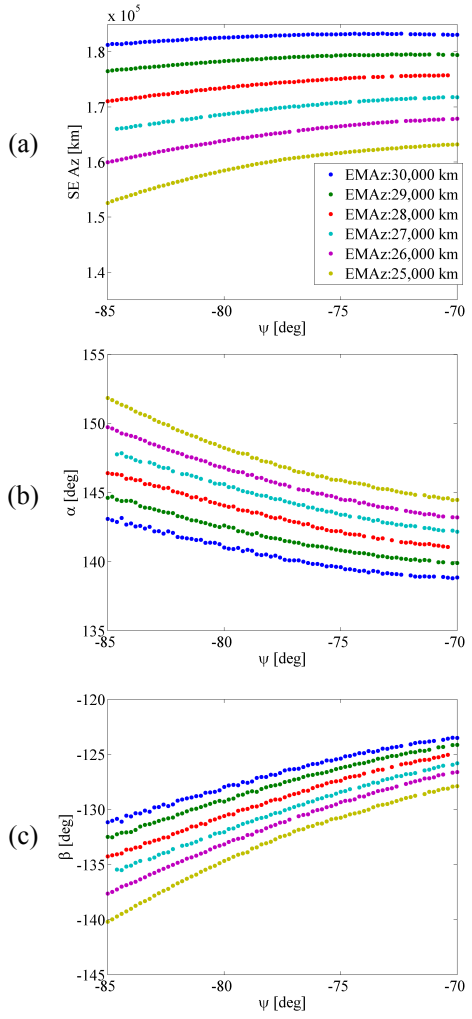

Fig. 5: Conditions for Maneuver-Free Transfers from EM halo orbits to SE halo orbits

obtaining useful phase plots. Generally, the desirable range for value of the hyperplane angle, ψ, is between $-85°$ and $-70°$ to achieve maneuver-free transfers from EML_2 halo orbits to SEL_2 halo orbits. Although the range varies as a function of the size of the departure halo orbit as well as the direction of the transfers, examination of a specific transfer type, such as EML_2-to-SEL_2 transfers, supplies useful information which is applicable to different transfer types. In Fig. 5, conditions for maneuver-free transfers are displayed. In the upper left plot, the required combinations of SEAz and EMAz at a specified value of ψ appear. Values for SEAz and ψ can then be estimated for a specific EMAz value from the figure.

Various types of phase plots are actually available that are associated with the hyperplane. However, this investigation demonstrates that only three phase plots are sufficient to compute a transfer. The three selected phase plots are summarized: (i) $\dot{x}_{ref}$ vs x_{ref}, (ii) z_{ref} vs x_{ref}, and (iii) $\dot{z}_{ref}$ vs z_{ref}. In each phase plot, Earth-Moon manifolds and Sun-Earth manifolds appear as closed curves due to the tube structure of manifolds. One key quantity for this process is the value of the Jacobi constant which is the only integral of motion in the CR3BP. The Jacobi constant indicates the energy level in the CR3BP. Thus, the Jacobi constant values corresponding to the intersecting Earth-Moon and Sun-Earth manifolds must be equal to achieve a maneuver-free transfer. In the Earth-Moon rotating frame, the Jacobi constant value corresponding to any point along the manifolds is equal to the value of the associated Earth-Moon halo orbit. However, the value is no longer constant after manifolds are transformed into the Sun-Earth rotating frame. Thus, the Jacobi constant value varies along the EM manifold curve in the phase plots, which are represented in terms of the Sun-Earth system. Three selected phase plots appear in Fig. 6. Red curves are unstable Earth-Moon manifolds and blue curves are stable Sun-Earth manifolds. A black circle on each phase plot indicates the manifold with a Jacobi constant value that is equal to the value along the entire set of Sun-Earth manifolds. The hyperplane guarantees the y_{ref} intersection. The intersection in the $\dot{x}_{ref}$ vs x_{ref} phase plot guarantees a corresponding match in $\dot{x}_{ref}$ and x_{ref}. Therefore, if the same intersecting manifolds possess an intersection in the other two phase plots, all states except $\dot{y}_{ref}$ are equal in value. Thus, it is necessary to introduce another phase plot related to $\dot{y}_{ref}$. However, rather than introducing another phase plot, Jacobi constant values are utilized in this process to 'match' the last component, i.e., $\dot{y}_{ref}$. In Fig. 6, the black circle clearly indicates the direction in which the red curve should be shifted in each phase plot. For example, in (a), it is clear that the red curve should be shifted to the left to move the black circle towards the blue curve.

V.III. Guidelines

The orientation of the Earth-Moon system determines the red curves in the phase plots for a fixed ψ. Thus, changing α and β shifts the red curves; changing α and β essentially modifies the location of the Moon in its orbit. The blue curves remain the same on the fixed hyperplane for a given value of SEAz. In plots in Fig. 7 demonstrate various shifts in the red curve in each phase plot is shifted to move the black circle toward the blue curve. The process to achieve the intersection in all three phase plots can be automated. The guidelines for the process are summarized as follows:

- Plots (b) and (c) in Fig. 5 correlate the values α and β to achieve a maneuver-free transfer for a desired set of EMAz and ψ. These results are useful to estimate the initial values for the design process.

- For the $\dot{x}_{ref}$ vs x_{ref} phase plot in Figs. 6 and 7, either α or β can be adjusted to shift the black circle closer to the blue curve.

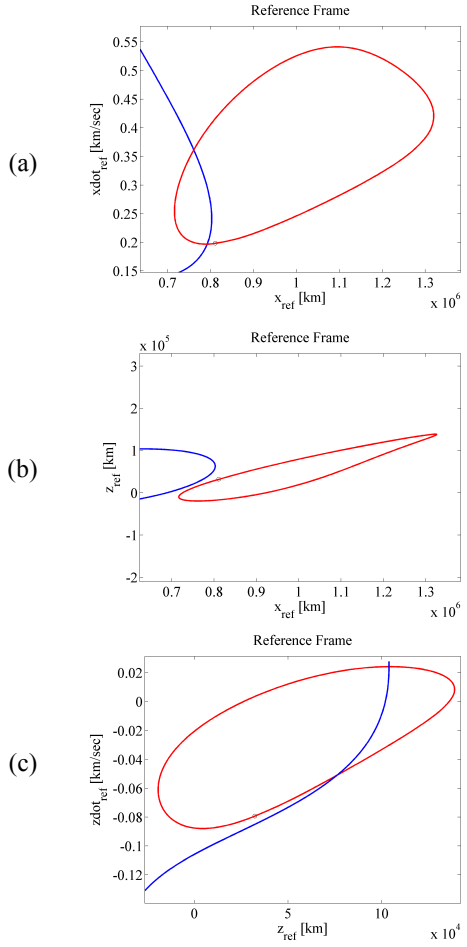

Fig. 6: Selected Phase Plots at Hyperplane: Blue curves are stable Sun-Earth manifolds. Red curves are unstable Earth-Moon manifolds. Black circles highlight the Earth-Moon manifold with the Sun-Earth Jacobi constant value.

- In the z_{ref} vs x_{ref} phase plot, most likely, the black circle does not intersect with the blue curve after an intersection is achieved in the $\dot{x}_{ref}$ vs x_{ref} phase plot. Thus, the black circle must be shifted to intersect with the blue curve by modifying the values of α and β. However, such an update also changes the $\dot{x}_{ref}$ vs x_{ref} phase plot. Maintaining the summation of α and β as a constant reduces the effect on the $\dot{x}_{ref}$ vs x_{ref} phase plot. For example, if α is shifted by 1°, β is altered by -1°. Physically, the adjustments in α and β change the location of the Moon by month and day, respectively. The change of β in the opposite direction reduces the shift of the state along the manifold. However, the shift reduction is small in the z-component.

- To achieve the intersection in the $\dot{z}_{ref}$ vs z_{ref} phase plot, the Sun-Earth amplitude Az value is adjusted. Since this adjustment affects other phase plots, both $\dot{x}_{ref}$ vs x_{ref} and z_{ref} vs x_{ref} phase plots are then be re-evaluated.

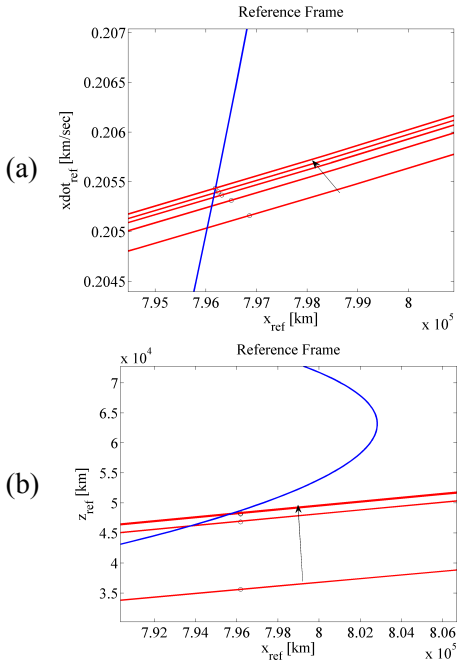

Fig. 7: Phase Plots as Trajectory Design Tools: Blue curves are stable Sun-Earth manifolds. Red curves are unstable Earth-Moon manifolds. Black circles highlight the Earth-Moon manifold with the Sun-Earth Jacobi constant value. The arrow indicates the direction in which the red curve shifts.

Phase plots that are produced at the completion of the process appear in Fig. 8. The black circle intersects with the blue curve in all the phase plots and a maneuver-free transfer is constructed. In Fig. 9, a black trajectory is computed with the state identified in the final phase plots. This trajectory links an unstable Earth-Moon manifold and approaches a Sun-Earth halo orbit. In this figure, the trajectory shifts from a stable Sun-Earth manifold to an unstable Sun-Earth manifold such that the path actually departs the SE halo orbit. It can be numerically corrected to remain on the SE halo orbit if desired.

These guidelines are sufficiently general to be applied to different transfer types including Earth-Moon L_2 halo orbits to/from Sun-Earth L_2 halo orbits and Earth-Moon L_2 halo orbits to/from Sun-Earth L_1 halo orbits. Sample results are summarized in Table 1. The first three examples in the table represent for the same transfer type, Earth-Moon L_2 to Sun-Earth L_2, but with different Earth-Moon Az values. As the Earth-Moon Az value changes, the Sun-Earth Az value and phase angles shift. However, since the changes are small, these values of SEAz and phase angles yield an initial guess for different Earth-Moon Az cases.

VI. TRANSFER SCENARIOS

Multiple departure scenarios are examined in this investigation. Since each scenario possesses its own advantages and disadvantages, one scenario may be

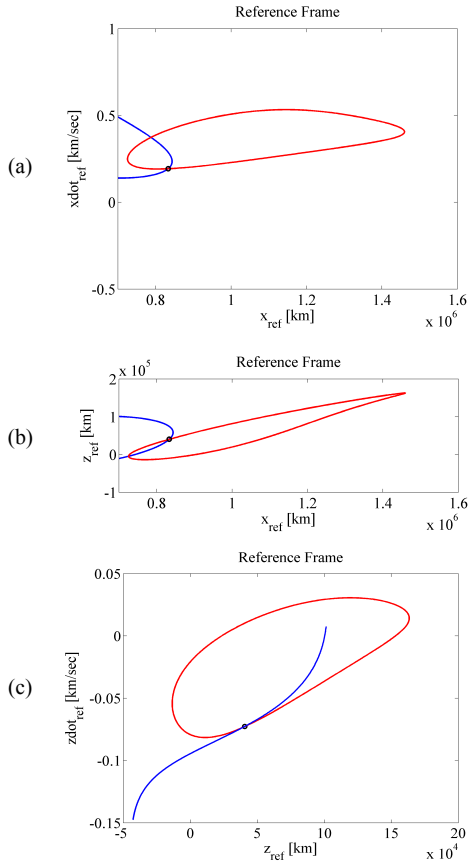

Fig. 8: Phase Plots for Earth-Moon L_2 Halo Orbit to Sun-Earth L_2 Halo Orbit Transfer

Table 1: Sample Results from the Procedure

Type	EMAz [km]	SEAz [km]	ψ [deg]
EML_2 to SEL_2	25,000	163,200	-70
EML_2 to SEL_2	26,000	167,900	-70
EML_2 to SEL_2	27,000	171,800	-70
SEL_2 to EML_2	25,000	163,900	70
EML_2 to SEL_1	25,000	162,600	110
SEL_1 to EML_2	25,000	163,000	-110
Type	α [deg]	i [deg]	β [deg]
EML_2 to SEL_2	144.47	5	-127.88
EML_2 to SEL_2	143.20	5	-126.60
EML_2 to SEL_2	142.17	5	-125.80
SEL_2 to EML_2	35.89	5	-52.68
EML_2 to SEL_1	-37.38	5	-124.68
SEL_1 to EML_2	-142.46	5	-55.59

better suited for certain mission requirements, and/or different destinations.

VI.I. Transfers via Sun-Earth Manifold

The first type of scenario to produce a Mars transfer utilizes a halo-to-halo transfer. This transfer scenario does not offer much flexibility in the departure date since the lunar location defined by α, i, and β must be specific as is apparent in Fig. 5. Based on the specified α and β values, multiple possible departure dates can be identified. However, the location of Mars at the arrival time limits the possible date ranges. The guidelines for computing successful transfers for this scenario are:

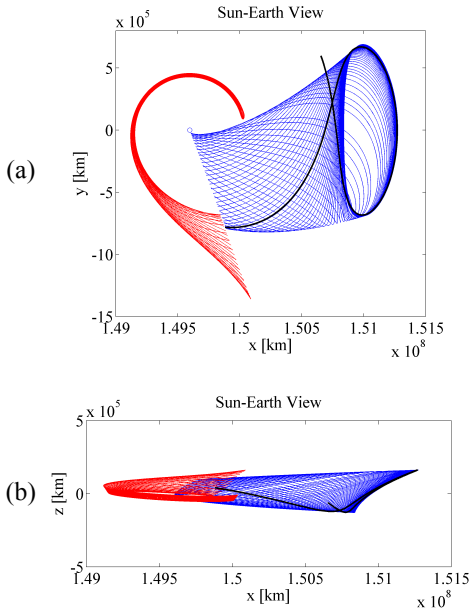

Fig. 9: Transfer from Earth-Moon L_2 Halo orbit to Sun-Earth L_2 Halo Orbit: EMAz = 25,000 km, SEAz = 163,200 km, ψ = -70 deg

- Possible departure dates are identified by comparing the angle combination (α, i, and β) with the phase angles corresponding to the ephemeris Moon. Multiple departure dates are available based on the angle information.

- Time-of-flight to Mars from a Sun-Earth manifold is estimated by computing a Hohmann transfer arc. Based on possible departure dates and the total time-of-flight, the appropriate locations of Mars at the arrival time are identified. It becomes apparent that most of the possible departure dates are not feasible due to the arrival conditions.

- Based on the estimated arrival date, the actual ephemeris location of Mars is obtained from the Mars database. Then, an osculating semi-major axis for the Mars orbit at the arrival time is computed. Re-computing the Hohmann transfer trajectory with the new semi-major axis improves the ΔV estimation to Mars.

- Previous contributers have exploited unstable Sun-Earth manifolds in the exterior region for departure arcs. However, in this scenario, stable Sun-Earth manifolds are exploited for the departure arcs, as viewed in Fig. 10, since the time-of-flight becomes significantly shorter. In addition, consistent with a two-body analysis, the energy

change or the ΔV value is slightly improved by the exploitation of stable manifolds. Also, the maneuver magnitude, i.e., ΔV, tends to be smaller when applied along the stable SE manifold near x-axis.

- Two maneuvers are applied by implementing a multiple shooting scheme. The first maneuver is applied to depart a Sun-Earth stable manifold. The location of the second maneuver is free to move along the path as required.

In Fig. 10, a transfer trajectory to Mars is constructed by modification of the conditions from the first case in Table 1. The ephemeris Mars orbit is displayed in red. Earth-Moon manifolds are also in red and Sun-Earth manifolds are plotted in blue. Results for a departure date of June 16 2022 appear in Table 2. The results demonstrate that the application of two maneuvers allows a reduction of the total ΔV from 3.869 km/sec to 3.495 km/sec. However, the increase in the time-of-flight from 277 days to 350 days is significant. In this example, the ΔV is reduced as the arrival approach to Mars becomes more tangential. The value of ΔV is higher than the estimated value from the planar Hohmann transfer which is 2.8 km/sec from the same location along the manifold. The balance of the total ΔV is mostly due to targeting the z-component of the ephemeris Mars position. The ephemeris Mars orbit is described with an the average inclination of 1.85°.[37] This small inclination has a significant impact on the ΔV value.

Table 2: Sun-Earth Manifold Transfer

Case	Departure Date	Total TOF [day]	ΔV [km/sec]
One Maneuver	June 16 2022	277	3.869
Two Maneuvers	June 16 2022	350	3.495

VI.II. Transfers via Earth-Moon Manifold

For the second scenario, an Earth-Moon manifold is also exploited to depart an Earth-Moon L_2 halo orbit. However, in this scenario, rather than shifting to a Sun-Earth manifold, the trajectory continues on the Earth-Moon manifold and returns to the vicinity of the Earth to gain the energy via an Earth gravity assist to leave the vicinity of the Earth. This scenario offers more flexibility in departure dates compared to the first example. To effectively accomplish a gravity assist and gain the promised flexibility, certain conditions must be satisfied. One of the conditions is a small perigee distance; another is a perigee location in the fourth quadrant of the Sun-Earth frame. Earth-Moon manifolds in the Sun-Earth rotating frame are plotted in red in Fig. 11. The hyperplane orientation is fixed at $\psi = -95°$; the angles α and β are each equal

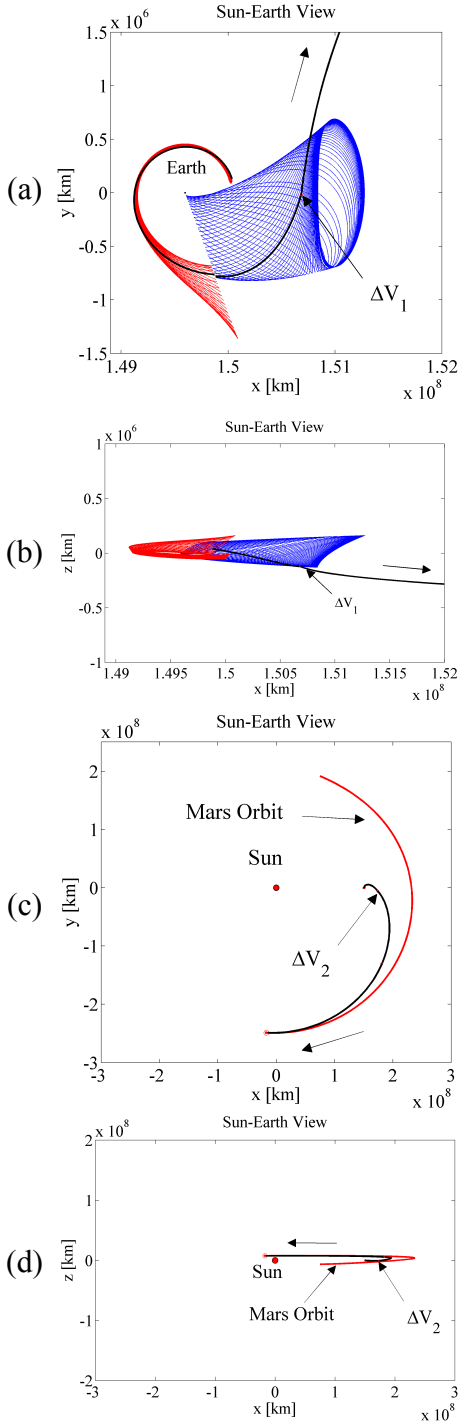

Fig. 10: Transfer from Earth-Moon L_2 to Mars via Sun-Earth Manifold: EMAz = 25,000 km, SEAz = 163,200 km, ψ = -70 deg

to 0°. To observe the flow of the manifolds passing through the hyperplane, the states at the hyperplane are integrated forward in the Sun-Earth system. The integrated trajectories appear in black in the figure. Since the behavior of these trajectories are complex, it is extremely challenging to predict how these trajectories vary as α, β, and ψ change. Therefore, thousands of combinations of α, β, and ψ are examined. The loca-

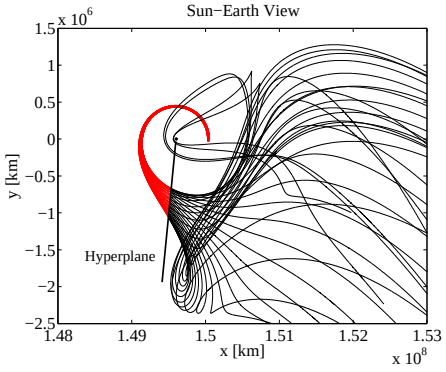

Fig. 11: Earth-Moon Manifolds in Sun-Earth Frame: $\psi = -95°$, $\alpha = \beta = 0°$

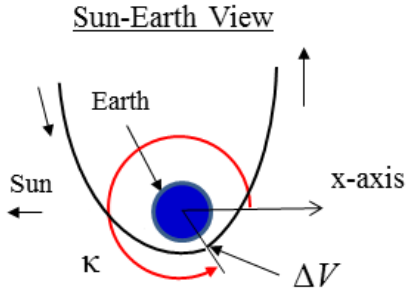

Fig. 12: Definition of κ: Perigee location

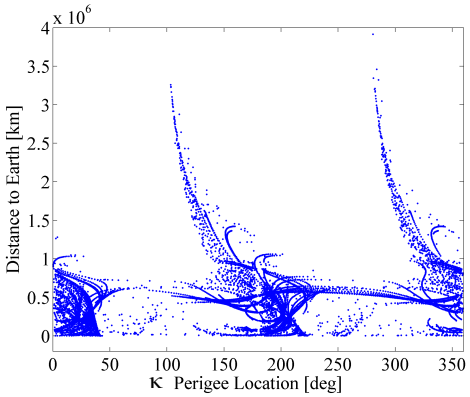

Fig. 13: Perigee Conditions

tion of perigee is defined by an angle κ as displayed in Fig. 12. The angle κ is measured from the Sun-Earth x-axis in the counter-clockwise direction.

The plot in Fig. 13 demonstrates perigee conditions corresponding to the Earth-Moon manifolds for hyperplane orientations in terms of ψ from 0° to 360°. The desired conditions recur periodically and offer possibilities for potentially promising flyby conditions. The guidelines to design transfers from the Earth-Moon L_2 orbit to Mars, through Earth-Moon manifolds, are summarized as follows:

- The perigee condition for the trajectory integrated in the Sun-Earth system must be verified. Generally, Earth passage distances that equal thousands of kilometers or even tens of thousands of kilometers are adequate results to be employed to a multiple shooting scheme. A maneuver is applied at the apogee location along the manifold to achieve the desired perigee condition as demonstrated in Fig. 14. If the perigee condition is not desirable, there are three options to improve the conditions. The first option is the selection of a different manifold. The second option involves the selection of a different α and β combination. Changing two angles in an open search for desirable perigee conditions without any guidance is not a good trajectory design strategy. However, by linking the ephemeris lunar location to the system model, the departure date automatically determines α, i, and β. The third option is the inclusion of a maneuver ΔV to improve the perigee conditions before the multiple shooting scheme is applied.

- To achieve a desirable flyby altitude, it is necessary to numerically correct the trajectory. A multiple shooting scheme supplies a robust algorithm for this task. A logical selection for the ΔV location to update perigee conditions is the apogee of the extended Earth-Moon manifold. In fact, the ΔV location varies by only a minor distance during the numerical corrections process. In Fig. 14, the near-Earth views of a Earth-Moon manifold transfer are plotted. The apogee maneuver location is indicated as ΔV_1.

- The second ΔV is applied at the corrected perigee location to depart for Mars. A departure ΔV is estimated by computing a Hohmann transfer arc. Since the spacecraft is very near the Earth, it is convenient to calculate a V_∞ value and use the two-body energy equation to estimate the ΔV at the perigee.

- When a transfer trajectory is computed, it is necessary to verify the location of Mars at the end of the time-of-flight. The best possible arrival date is determined by identifying the best arrival Mars' location from the possible locations. The possible dates do not necessarily supply the desirable targeted location. Thus, the initial date requires modification to improve Mars' location at arrival. This modification obviously shifts the orientation of the Earth-Moon system, and results in a change in the flyby conditions at perigee. To minimize the change, the departure date is varied by the increment of approximately 29.5 days, i.e., the lunar synodic period. Thus, the Moon remains approximately at the same location in the Sun-Earth frame.

- After one possible arrival Mars' location is determined, additional potential final Mars' locations are identified by varying the final time with the

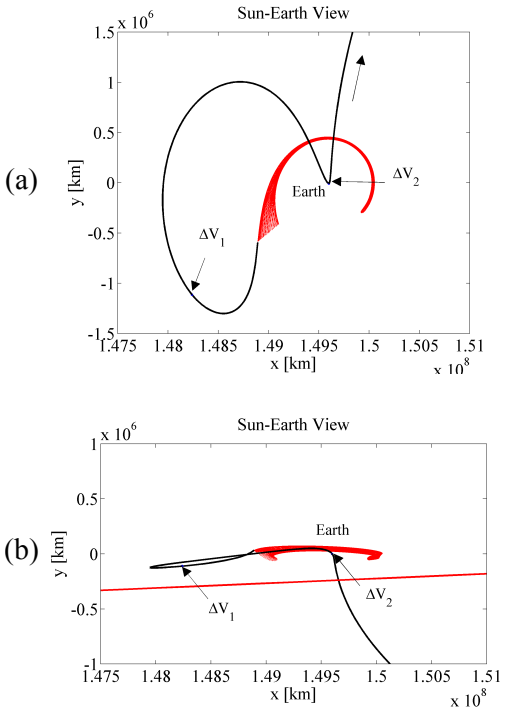

Fig. 14: Earth-Moon Manifold Transfer from Earth-Moon L_2: Views near the Earth

step size corresponding with the Mars' synodic period which is approximately 780 days.

- Generally, additional ΔV locations lowers the total ΔV requirements. A suggested initial guess for the maneuver location is the maximum y-excursion along the transfer trajectory. The final location of the maneuver after numerical corrections tends to remain close to this region even without a location constraint as demonstrated in Fig. 15.

- In this transfer scenario, the transfer arc associated with a Hohmann transfer is not a sufficiently accurate approximation to serve as an adequate initial guess. The initial guess can be improved by adjusting the ΔV before the multiple shooting scheme is applied.

The results from these sample cases appear in Table 3. The EMAz amplitude is 25,000 km. The departure opportunity recurs every two years. The time spent near Earth until the second maneuver is approximately 160 days because of the low energy dynamics associated with the manifold trajectories. The flyby altitude is selected to be equal to 1,000 km. The total ΔV is significantly lower than the first scenario via Sun-Earth manifolds. However, the total time of flight is $100-200$ days longer than the first scenario.

Similar guidelines apply to EM manifold transfers from EML_1 halo orbits. In this case, unstable EM

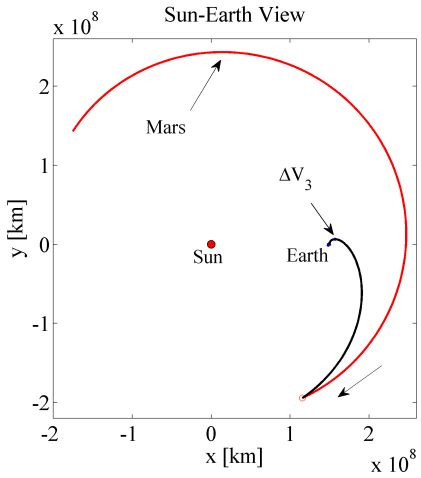

Fig. 15: Earth-Moon Manifold Transfer from Earth-Moon L_2: The location of the third maneuver is indicated by ΔV_3.

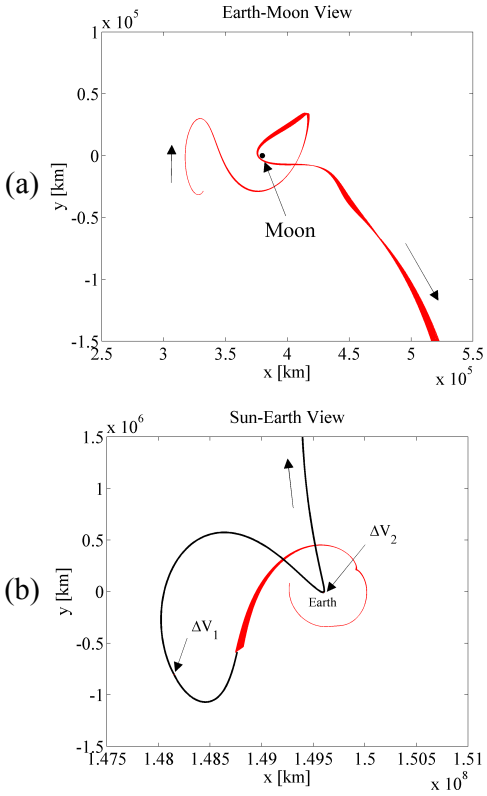

Fig. 16: Earth-Moon Manifold Transfer from Earth-Moon L_1

manifolds are propagated towards the Moon to escape to the exterior region as demonstrated in Fig. 16(a). The general transfer paths are similar to the transfers from the L_2 side as displayed in Fig. 16(b). Table 3 lists sample results. As in the L_2 cases, the time spent until the second maneuver is approximately 160 days.

VI.III. Direct Transfers

The third scenario is a direct transfer that does not exploit manifolds. In this case, a maneuver is applied to

Table 3: Earth-Moon Manifold Transfer: EMAz = 25,000 km; Leg 1 is from the departure from EM halo to ΔV_1. Leg 2 is from ΔV_1 to ΔV_2. Leg 3 is from ΔV_2 to ΔV_3.

Departure Date:		Leg 1	Leg 2	Leg 3	Total
EML_2 Departure					
May 28 2026	TOF [days]	75	90	35	424
	ΔV [km/sec]	0.020	0.570	0.331	0.921
July 3 2028	TOF [days]	75	77	45	380
	ΔV [km/sec]	0.003	0.450	0.307	0.759
September 9 2030	TOF [days]	74	83	26	475
	ΔV [km/sec]	0.010	0.394	1.006	1.410
EML_1 Departure					
May 16 2026	TOF [days]	89	73	41	441
	ΔV [km/sec]	0.006	0.391	0.500	0.897
June 21 2028	TOF [days]	90	69	50	388
	ΔV [km/sec]	0.030	0.517	0.254	0.802
September 26 2030	TOF [days]	90	71	46	487
	ΔV [km/sec]	0.020	0.463	0.207	0.690

depart an EML_2 halo orbit and target a close flyby at Earth. In Fig. 17, a departure trajectory in the Earth-Moon frame is plotted in red. Since this scenario does not exploit manifolds, the time-of-flight is reduced significantly. However, it requires a significant amount of ΔV to depart an EML_2 halo orbit. The corresponding guidelines are:

- A maneuver is applied at the location where the y-component is zero and the z-component is a maximum, in Fig. 17. This maneuver allows the spacecraft to move along the trajectory and pass close to the Earth. The magnitude of the ΔV is adjusted to achieve a desired perigee altitude.

- The propagated trajectory is transformed into the Sun-Earth frame by use of the phase angles, α, i, and β. The direct transfers offer more flexibility on selecting α and β than other scenarios. The angles (i.e., the location of the Moon in its orbit) are selected so that the perigee occurs in the fourth quadrant in the Sun-Earth frame for promising flyby conditions. In Fig. 18(a), the x-y projection of the transformed trajectory appear in red.

- The process to compute the transfer trajectory from the Earth flyby to Mars is the same as the procedure in the second scenario.

Table 4 summarizes the results from the example cases. The EMAz is 25,000 km. This scenario delivers spacecraft to Mars in significantly shorter time frame than the second scenario. In Fig. 18(a), the red arc is the trajectory computed in the Earth-Moon system. The time-of-flight for the arc is only about 6 days. However, the ΔV cost is higher due to the fact that the maneuver to depart the EM halo orbit is larger. Approximately 925 m/sec is required to depart a halo orbit and reach a suitable perigee point, 1,000 km altitude.

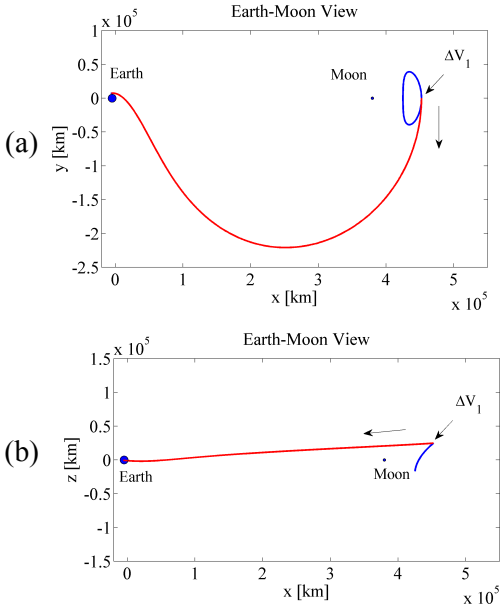

Fig. 17: Direct Transfer from Earth-Moon L_2: ΔV is applied to leave a halo orbit.

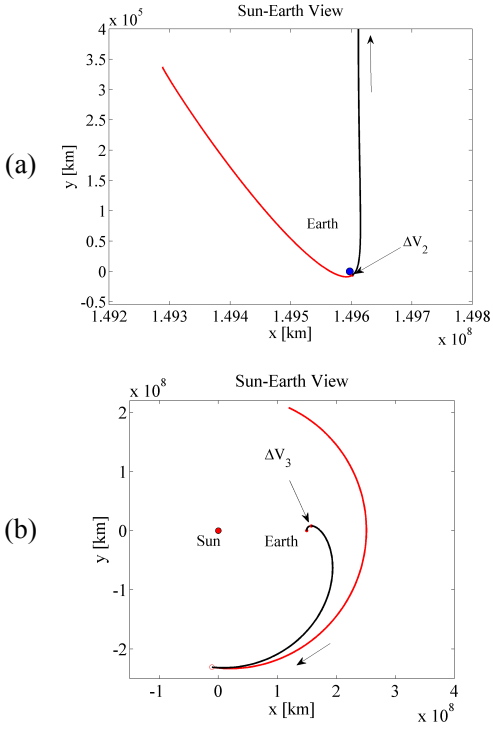

Fig. 18: Direct Transfer from Earth-Moon L_2: Two additional ΔVs are applied to reach Mars.

The similar guidelines apply to transfers from L_1 halo orbits. The location of the first maneuver to depart an L_1 halo orbit is also where the y-component is zero, but the z-component is a minimum as plotted in Fig. 19. The size of the ΔV is still significant, e.g., 575 m/sec to depart an L_1 halo orbit with 25,000 km Az, Table 4.

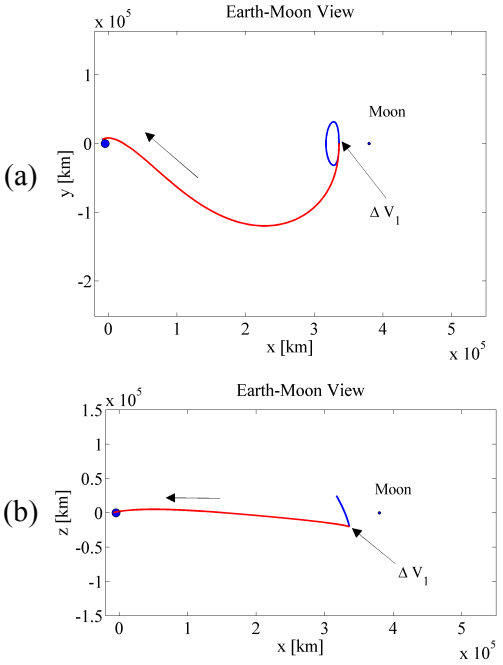

Fig. 19: Direct Transfer from Earth-Moon L_1: ΔV is applied to leave a halo orbit.

Table 4: Direct Transfers: EMAz = 25,000 km; Leg 1 is from the departure from EM halo to the Earth flyby. Leg 2 is from the Earth flyby to ΔV_3. Leg 3 is from ΔV_3 to Mars.

Departure Date:		Leg 1	Leg 2	Leg 3	Total
EML_2 Departure					
November 4 2026	TOF [days]	6	44	222	272
	ΔV [km/sec]	0.925	0.581	0.088	1.593
December 11 2028	TOF [days]	6	46	205	257
	ΔV [km/sec]	0.925	0.504	0.806	2.235
March 18 2031	TOF [days]	6	43	294	343
	ΔV [km/sec]	0.925	0.512	0.013	1.450
EML_1 Departure					
November 4 2026	TOF [days]	5	43	229	277
	ΔV [km/sec]	0.575	0.591	0.049	1.215
December 11 2028	TOF [days]	5	39	182	226
	ΔV [km/sec]	0.575	0.631	0.217	1.423
January 18 2031	TOF [days]	5	38	150	193
	ΔV [km/sec]	0.575	0.450	0.550	1.575

VI.IV. Transfers with Lunar Flyby

The fourth scenario is a transfer that exploits manifolds and a lunar flyby. Instead of applying a maneuver to depart an L_2 halo orbit and obtain Earth flyby conditions, a maneuver is applied at the perilune along an unstable EM manifold approaching the Moon to obtain Earth flyby conditions. Once the Earth flyby conditions are achieved, the guidelines are the same as the third scenario, direct transfers. The time-of-flight from an L_2 halo orbit to Earth is approximately 20 days for the example results listed in Table 5. Note that the selected EMAz is 5,000 km. The value of the ΔV at the lunar flyby increases as a function of the EMAz. However, an additional maneuver to depart a halo orbit reduces the amount of ΔV to achieve the Earth flyby for larger halo orbits.[42] Table 6 summarizes sample cases with an additional maneuver. In this scenario, the total maneuver to achieve the Earth flyby from the EML_2 orbit is 329 m/sec rather than 925 m/sec in the direct transfer scenario.

Table 5: EM Manifold Transfers with Lunar Flyby: EMAz = 5,000 km; Leg 1 is from the departure from EML_2 to the Earth flyby. Leg 2 is from the Earth flyby to ΔV_3. Leg 3 is from ΔV_3 to Mars.

Departure Date:		Leg 1	Leg 2	Leg 3	Total
October 21 2026	TOF [days]	20	39	233	292
	ΔV [km/sec]	0.236	0.612	0.074	0.923
November 26 2028	TOF [days]	20	39	195	253
	ΔV [km/sec]	0.236	0.590	0.165	0.991
January 3 2031	TOF [days]	20	38	160	218
	ΔV [km/sec]	0.236	0.416	0.591	1.243

Table 6: Direct Transfers with Lunar Flyby: EMAz = 25,000 km; Leg 1 is from the departure from EM halo to the lunar flyby. Leg 2 is from the lunar flyby to the Earth flyby. Leg 3 is from the Earth flyby to ΔV_4. Leg 4 is from ΔV_4 to Mars.

Departure Date:		Leg 1	Leg 2	Leg 3	Leg 4	Total
EML_2 Departure						
October 25 2026	TOF [days]	10	5	39	230	284
	ΔV [km/sec]	0.079	0.250	0.650	0.102	1.082
December 1 2028	TOF [days]	10	5	40	195	249
	ΔV [km/sec]	0.079	0.250	0.666	0.155	1.150
January 7 2031	TOF [days]	10	5	40	148	202
	ΔV [km/sec]	0.079	0.250	0.487	0.557	1.373
EML_1 Departure						
November 2 2026	TOF [days]	2	3	34	231	271
	ΔV [km/sec]	.230	0.270	0.495	0.324	1.319
December 9 2028	TOF [days]	2	3	35	175	215
	ΔV [km/sec]	0.230	0.270	0.498	0.260	1.258
January 16 2031	TOF [days]	2	3	36	170	210
	ΔV [km/sec]	0.230	0.270	0.304	1.038	1.842

VI.V. Transition to Higher-Fidelity Model

To evaluate the functionality of the blended model, results from each transfer scenario are transitioned to a higher-fidelity model with ephemeris Sun, Earth, Moon, and Mars. Sample results from the ephemeris model are listed in Table 7. Departure dates predicted from the blended model are reasonable estimates for the ephemeris model. In the direct transfer case, the departure date is shifted by one day after the transition. Also, time-of-flight values are estimated well by the blended model. The total ΔV values generally increase after the transition, but the increases are within a few hundred m/s. A sample direct transfer result is displayed in Fig. 20; the path originates from an EML_2 halo orbit. According to Table 7, the EMAz increases from 25,000 km to 46,000 km after the transition to the ephemeris model. The increase in Az is apparent in the figure. The original EM halo orbit is in blue, and the transfer path is plotted in red in Figs. 20(a)-(b). The trajectory in the ephemeris model is plotted in magenta. In Fig. 20(c) the trajectory from

the blended model is plotted in black, and the trajectory from the ephemeris model is plotted in magenta in the Sun-Earth rotating frame. The magenta trajectory follows a similar path to the black trajectory.

Table 7: Comparison of Results, BCR3BP and Ephemeris: EMAz for the ephemeris case is the mean of maximum Az values of the quasi-halo orbit. (*: direct case with an additional maneuver)

Case	EMAz [km]	Departure Date	TOF [day]	ΔV [km/sec]
SE Transfer BCR3BP	25,000	June 16 2022	350	3.495
SE Transfer Ephemeris	25,000	June 16 2022	350	3.645
L_2 EM BCR3BP	25,000	July 3 2028	380	0.759
L_2 EM Ephemeris	33,000	July 3 2028	376	0.852
L_2 Direct BCR3BP	25,000	November 4 2026	272	1.593
L_2 Direct Ephemeris	46,000	November 3 2026	262	1.631
L_2 Lunar BCR3BP	5,000	November 26 2028	253	0.991
L_2 Lunar Ephemeris	6,000	November 26 2028	250	1.096
L_2 Lunar* BCR3BP	25,000	December 1 2028	249	1.150
L_2 Lunar* Ephemeris	27,000	December 1 2028	249	1.413

VII. CONCLUSIONS

General design procedures for four transfer scenarios from Earth-Moon L_1/L_2 halo orbits to Mars are developed. In addition, to exploit Sun-Earth manifolds as an option to transfer to Mars, a general procedure to compute maneuver-free transfers between Earth-Moon L_2 halo orbits to Sun-Earth L_2 halo orbits is developed. This procedure is sufficiently general to support the construction of maneuver-free transfers between Earth-Moon L_2 halo orbits from/to Sun-Earth L_1/L_2 halo orbits. The model of a five-body regime in which gravitational bodies are Sun, Earth, Moon, and Mars is constructed by blending Earth-Moon and Sun-Earth systems with the ephemeris Mars location. Then, the results produced by the blended model are transitioned to a higher-fidelity model with ephemeris Sun, Earth, Moon, ans Mars. The comparison of the results demonstrate that the trajectories computed from the blended model produce a reasonable guess to be transitioned to the ephemeris model.

VIII. ACKNOWLEDGEMENTS

The authors appreciate the support from the School of Aeronautics and Astronautics as well as the School of Engineering Education. Portions of the work were completed under NASA Grant No. NNX13AE55G.

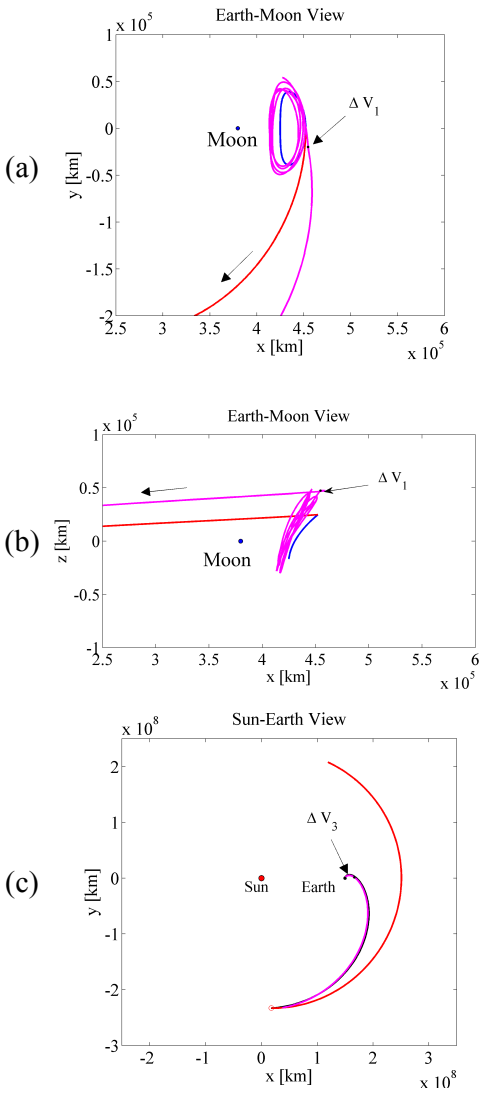

Fig. 20: Direct Transfer from Earth-Moon L_2 Libration Orbit: EMAz $= 25,000$ km. The departure date is November 4 2026. The trajectory in the ephemeris model is plotted in magenta.

REFERENCES

[1]R. W. Farquhar, "The Utilization of Halo Orbits in Advanced Lunar Operations," *NASA Technical Note*, vol. NASA TN D-6365, 1971.

[2]M. Woodard, D. Folta, and D. Woodfork, "ARTEMIS: The First Mission to the Lunar Libration Points," (21st International Symposium on Space Flight Dynamics, Toulouse, France), September 28 - October 2 2009.

[3]J. Hopkins, "Fastnet: Early Telerobotic Exploration of the Lunar Farside by astronauts at Earth-Moon l_2," Future In-Space Operations colloquium, November 14 2012.

[4]K. C. Howell, B. T. Barden, and M. W. Lo, "Application of Dynamical Systems Theory to Trajectory Design for a Libration Point Mission," *The Journal of the Astronautical Sciences*, vol. 45, pp. 161–178, April-June 1997.

[5]D. Burnett, B. Barraclough, R. Bennet, M. Neugebauer, L. Oldham, C. Sasaki, D. Sevilla, N. Smith, E. Stansbery, D. Sweetnam, and R. Wiens, "The Genesis Discovery Mission: Return of Solar Matter to Earth," *Space Science Reviews*, vol. Vol. 105, p. 509, 2003.

[6]K. Howell, B. Barden, R. Wilson, and M. Lo, "Trajectory Design Using a Dynamical Systems Approach with Application to Genesis," Paper No. AAS 97-709, (AIAA/AAS Astrodynamics Specialist Conference, Sun Valley, Idaho), AAS/AIAA, August 1997.

[7]M. W. Lo, B. G. Williams, W. E. Bollman, D. Han, R. A. Corwin, P. E. Hong, K. C. Howell, B. Brian, and R. Wilson, "Genesis Mission Design," Paper No. AIAA-1998-4468, (AIAA/AAS Astrodynamics Specialist Conference and Exhibit, Boston, Massachusetts), AIAA, August 1998.

[8]D. Folta and K. Richon, "Libration Orbit Mission Design at L2: A Map and NGST Perspective," Paper No. AIAA 98-4469, (AIAA/AAS Astrodynamics Specialist Conference, Boston, MA), August 10-12 1998.

[9]H. Franz, P. Sharer, K. Ogilvie, and M. Desch, "Wind Nominal Mission Performance and Extended Mission Design," *Journal of the Astronautical Sciences*, vol. 49, pp. 145–167, 2001.

[10]G. Gómez, W. Koon, M. Lo, J. Marsden, S. Ross, and J. Masdemont, "Invariant Manifolds, the Spatial Three-Body Problem and Petit Grand Tour of Jovian Moons," *Libration Point Orbits and Application*, pp. 587–601, 2003.

[11]G. Gómez, W. Koon, M. Lo, J. Marsden, J. Masdemont, and S. Ross, "Connecting Orbits and Invariant Manifolds in the Spatial Restricted Three-Body Problem," *Nonlinearity*, vol. 17, no. 5, p. 1571, 2004.

[12]W. S. Koon, M. W. Lo, J. E. Marsden, and S. D. Ross, "Constructing a Low Energy Transfer between Jovian Moons," *Contemporary Mathematics*, pp. 129–145, 2002.

[13]W. S. Koon, M. W. Lo, J. E. Marsden, and S. D. Ross, "Shoot the Moon," Paper No. AAS 00-166, (AAS/AIAA Space Flight Mechanics Meeting, Florida), January 2000.

[14]W. S. Koon, M. W. Lo, J. E. Marsden, and S. D. Ross, "Low Energy Transfer to the Moon," *Celestial Mechanics and Dynamical Astronomy*, pp. 63–73, 2001.

[15]J. Parker and M. Lo, "Shoot the Moon 3D," Paper No. AAS 05-383, (AAS/AIAA Astrodynamics Specialists Conference, Lake Tahoe, California), August 2005.

[16]J. Parker, "Families of Low Energy Lunar Halo Transfers," Paper No. AAS 06-132, (AAS/AIAA Spaceflight Mechanics Meeting, Tampa, Florida), January 2006.

[17]J. S. Parker and G. H. Born, "Modeling a Low-Energy Ballistic Lunar Transfer Using Dynamical Systems Theory," *Journal of Spacecraft and Rockets*, vol. 45, no. 6, pp. 1269–1281, 2008.

[18]J. Parker, "Low-Energy Ballistic Transfers to Lunar Halo Orbits," Paper No. AAS 09-443, (AAS/AIAA Astrodynamics Specialist Conference, Pittsburgh, Pennsylvania), August 2009.

[19]K. C. Howell and M. Kakoi, "Transfers between the Earth-Moon and Sun-Earth Systems Using Manifolds and Transit Orbits," *Acta Astronautica*, vol. 59, pp. 367–380, 2006.

[20]E. Canalias and J. Masdemont, "Computing Natural Transfers between Sun-Earth and Earth-Moon Lissajous Libration Point Orbits," *Acta Astronautica*, vol. 63, pp. 238–248, 2008.

[21]K. Howell, M. Beckman, C. Patterson, and D. Folta, "Representations of Invariant Manifolds for Applications in Three-Body Systems," *The Journal of the Astronautical Sciences*, vol. 54, no. 1, pp. 69–93, 2006.

[22]G. Mingotti, F. Topputo, and F. B. Zazzera, "Attainable Sets in Space Mission Design: a Method to Define Low-Thrust, Invariant Manifold Trajectories," Paper No. AAS-12-137, (AAS/AIAA Space Flight Mechanics Meeting,Charleston,South Carolina), January 2012.

[23]P. Zhang, J. Li, H. Baoyin, and G. Tang, "A Low-Thrust Transfer between the Earth-Moon and Sun-Earth Systems Based on Invariant Manifolds," *Acta Astronautica*, 2013.

[24]M. W. Lo and S. D. Ross, "The Lunar L_1 Gateway: Portal to the Stars and Beyond," (AIAA Space 2001 Conference and Exposition, Albuquerque, New Mexico), AIAA, August 2001.

[25]M. W. Lo, "The Interplanetary Superhighway and the Origins Program," *IEEE Aerospace Conference Proceedings*, vol. 7, pp. 3543–3562, March 9-16 2002.

[26]G. P. Alonso, "The Design of System-To-System Transfer Arcs Using Invariant Manifolds in the Multi-Body Problem," Ph.D. Dessertation, School of Aeronautics and Astronautics, Purdue University, West Lafayette, Indiana, December, 2006.

[27]F. Topputo, M. Vasile, and A. E. Finzi, "An Approach to the Design of Low Energy Interplanetary Transfers Exploiting Invariant Manifolds of the Restricted Three-Body Problem," Paper No. AAS 04-245, (AAS/AIAA Space Flight Mechanics Conference,Maui, Hawaii), February 2004.

[28]F. Topputo, M. Vasile, and F. B. Zazzera, "A Hybrid Optimization of the Low Energy Interplanetary Transfers Associated to the Invariant Manifolds of the Restricted Three-Body Problem," Paper No. IAC-04-A.6.06, (International Astronautical Congress, Vancouver, Canada), October 2004.

[29]M. Nakamiya, D. Scheeres, H. Yamakawa, and M. Yoshikawa, "A Study of Earth–Mars Interplanetary Transfer Using Spaceports at the Lyapunov Orbits of Sun-Earth and Sun-Mars System," Paper No. IAC-08-A5.3.07, (International Astronautical Congress, Glasgow, Scotland), October 2008.

[30]M. Nakamiya, H. Yamakawa, D. Sheeres, and M. Yoshikawa, "Interplanetary Transfers between Halo Orbits: Connectivity between Escape and Capture Trajectories," *Journal of Guidance, Control, and Dynamics*, vol. 33, pp. 803–313, May-June 2010.

[31]G. Mingotti and P. Gurfil, "Mixed Low-Thrust and Invariant-Manifold Transfers to Unstable Distant Prograde Orbits around Mars," Paper No. AIAA 2010-7832, (AAS/AIAA Astrodynamics Specialist Conference, Toronto, Ontario Canada), August 2010.

[32]G. Mingotti, F. Topputo, and F. B. Zazzera, "Invariant-Manifold, Low-Thrust Transfers to Low Mars Orbits," Paper No. IAC-10-C1.9.1, (International Astronautical Congress, Prague, Czech Republic), September-October 2010.

[33]G. Mingotti, F. Topputo, and F. B. Zazzera, "Earth-Mars Transfers with Ballistic Escape and Low-Thrust Capture," *Celestial Mechanics and Dynamical Astronomy*, vol. 110, pp. 169–188, June 2011.

[34]C. Finocchietti, P. Pergola, and M. Andrenucci, "Venus Transfer Design by Combining Invariant Manifolds and Low–Thrust Arcs," *Acta Astronautica*, 2013.

[35]A. Haapala and K. Howell, "Trajectory Design Strategies Applied to Temporary Comet Capture Including Poincaré Maps and Invariant Manifolds," *Celestial Mechanics and Dynamical Astronomy*, pp. 1–25, 2013.

[36]D. C. Folta, M. A. Woodard, T. A. Pavlak, A. F. Haapala, and K. C. Howell, "Earth-Moon Libration Point Orbit Stationkeeping: Theory, Modeling, and Operations," *Acta Astronautica*, 2013.

[37]J. E. Prussing and B. A. Conway, *Orbital Mechanics*. New York: Oxford University Press, first ed., 1993.

[38]J. Stoer and R. Bulirsch, *Introduction to Numerical Analysis*. New York: Springer-Verlag, 1980.

[39]T. A. Pavlak and K. C. Howell, "Evolution of the Out-of-Plane Amplitude for Quasi-Periodic Trajectories in the Earth–Moon System," *Acta Astronautica*, vol. 81, no. 2, pp. 456–465, 2012.

[40]M. Vaquero and K. C. Howell, "Design of Transfer Trajectories between Resonant Orbits in the Earth-Moon Restricted Problem," *Acta Astronautica*, 2013.

[41]T. A. Pavlak, "Trajectory Design and Orbit Maintenance Strategies in Multi-Body Dynamical Regimes," Ph.D. Dessertation, School of Aeronautics and Astronautics, Purdue University, West Lafayette, Indiana, December, 2013.

[42]D. Folta, P. T., H. A., and H. K., "Preliminary Considerations for Access and Operations in Earth-Moon L1/L2 Orbits," Paper No. AAS 13-339, (AAS/AIAA Space Flight Mechanics Meeting, Kauai, Hawaii), February 10-14 2013.